Two-Phase Continuum Models for Geophysical Particle-Fluid Flows

Time-dependent measurements for incipient bed load discharge on shallow open channel flows

Guilherme H. FIOROT

supervisors :
Pascal DUPONT
Geraldo de F. MACIEL

LGCGM - INSA de Rennes & PPGEM - UNESP de Ilha Solteira

March 14-18, 2016

General framework

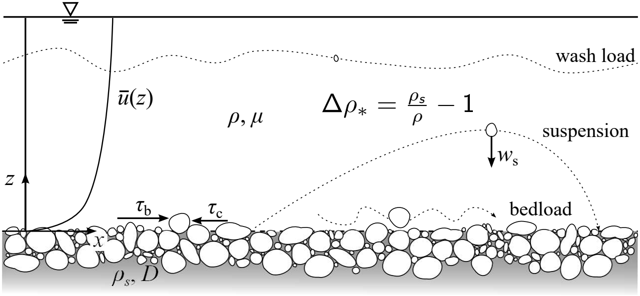

q_0 ; u_0 ; h_0 ;

$\rightarrow \tau_b$; u_* ;

$u_* > u_{*c}$:

Transport !

Shields number

$\mathrm{Sh} = u_*^2/(\Delta\rho_* g D)$;

Transport

$\rightarrow q_* = A(\mathrm{Sh} - \mathrm{Sh}_c)^B$.

(Shields, 1936; Paphitis, 2001; Beheshti and Ataie-Ashtiani, 2008)
(Meyer-Peter and Müller, 1948; Wong and Parker, 2006)

Dimensionless analysis

Reynolds :	$\mathrm{Re} = 4\dfrac{u_0 h_0}{\nu}$	flow dynamics ;
Froude :	$\mathrm{Fr} = \dfrac{u_0}{\sqrt{g h_0 \cos\theta}}$	flow hydraulic regimen ;
Shields :	$\mathrm{Sh} = \dfrac{u_*^2}{\Delta\rho_* g D}$	particles initiation of motion ;
Particle Reynolds :	$\mathrm{Re}_p = \dfrac{u_0 D}{\nu}$	particle-flow interaction ;
Stokes :	$\mathrm{St} = \dfrac{T_p}{T_f}$	particles-flow interaction ;
Particle Froude :	$\mathrm{Fr}_p = \dfrac{u_0}{\sqrt{gD}}$	flow capacity of transport ;
Rouse : (suspension or movability)	$\dfrac{w_s}{\kappa u_*}; \dfrac{w_s}{u_*}; \dfrac{u_*}{w_s}$	dominant mode of sediment transport ;

Dimensionless analysis

Reynolds :	$\mathrm{Re} = 4\frac{u_0 h_0}{\nu}$	flow dynamics ;
Froude :	$\mathrm{Fr} = \frac{u_0}{\sqrt{g h_0 \cos\theta}}$	flow hydraulic regimen ;
Shields :	$\mathrm{Sh} = \frac{u_*^2}{\Delta\rho_* g D}$	particles initiation of motion ;
Particle Reynolds :	$\mathrm{Re}_p = \frac{u_0 D}{\nu}$	particle-flow interaction ;
Stokes :	$\mathrm{St} = \frac{T_p}{T_f}$	particles-flow interaction ;
Particle Froude :	$\mathrm{Fr}_p = \frac{u_0}{\sqrt{gD}}$	flow capacity of transport ;
Rouse : (suspension or movability)	$\frac{w_s}{\kappa u_*} ; \frac{w_s}{u_*} ; \frac{u_*}{w_s}$	dominant mode of sediment transport ;

Non-stationary transport - Turbulence

$$u_* \propto u_0$$

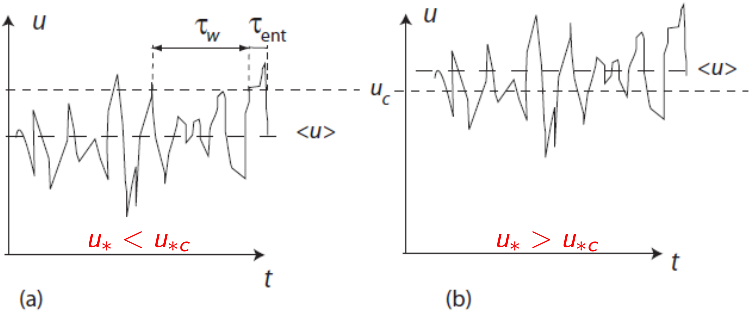

Figure 1 – Fluctuations of the instantaneous velocity around the mean value. Particle entrainment occurs sporadically. (Ancey et al., 2008).

Non-stationary transport - Grain-size distribution

Heterogeneous

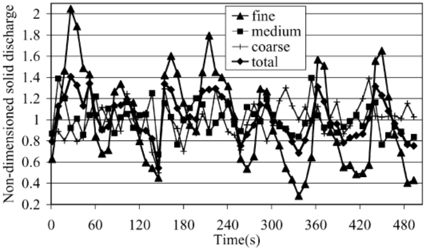

Fig. 17. Solid discharges of fine, medium, coarse materials and total (run 4)

Homogeneous

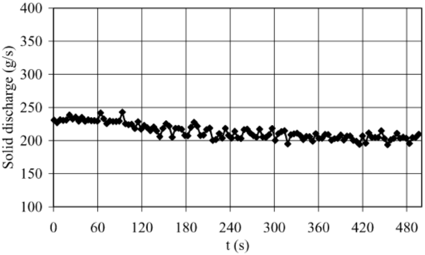

Fig. 18. Time series of solid discharge for the uniform material (run 13)

Figure 2 – Solid discharges of materials with different granulometry (Frey et al., 2003).

Non-stationary transport - Flow instabilities

Free surface instabilities

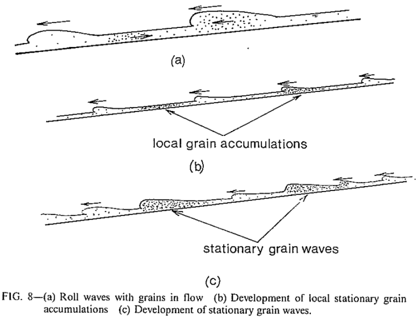

Figure 3 – Evolution of roll waves and sediment transport (Davies, 1990).

& Bedforms

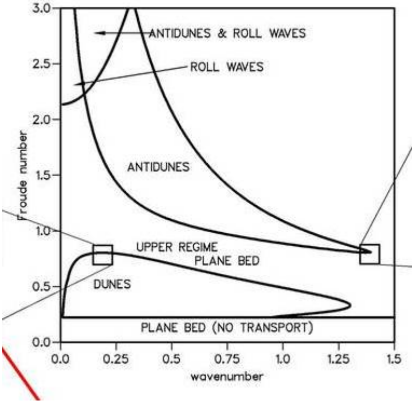

Figure 4 – Comparison of stability lines for roll waves and bedforms (Colombini and Stocchino, 2005).

Main objective

Non-stationary sediment transport

Experimentally study time-dependent effects on sediment transport for runoff flows.

Main objective

Non-stationary sediment transport

Experimentally study time-dependent effects on sediment transport for runoff flows.

Close to threshold cases :

Shields number
$\mathrm{Sh} < 2.5\mathrm{Sh}_c$;

(Recking et al., 2009)

Turbulence effects :

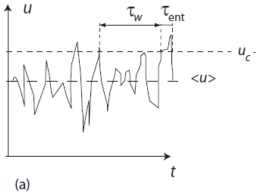

Experimental project

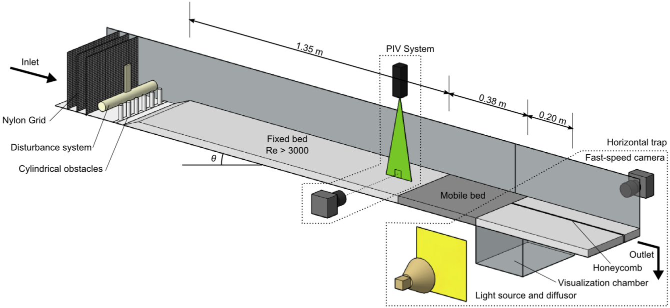

Figure 5 – Sketch of experimental setup.

- shallow water flow $h_0/l \ll 1$;
- PIV method for local flow dynamics measurements ;
- contact needle for global measurements ;
- combined shadowgraph and PTV methods for local sediment transport measurements ;

Test sand

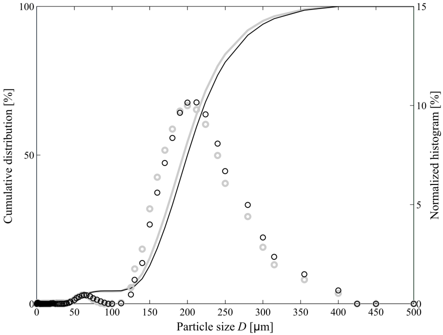

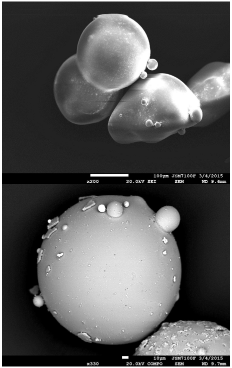

Figure 6 – Histogram for particles used in experiments and MEV images.

- non-cohesive ;
- regular shape ;
- $0.15 < D < 0.25$ mm ;
- $\mathrm{Sh}_c = 0.062$;
- favorable to bedload (given the exp. limitations, $w_s \approx 2\mathrm{cm/s}$) ;

Dimensionless parameters

Dimensionless	Range	Interpretation
Re	$3000 < \mathrm{Re} < 4000$	Turbulent (close to transition) ;
Fr	$1.1 < \mathrm{Fr} < 1.5$	Torrential flows
Sh	$0.068 < \mathrm{Sh} < 0.165$	particles initiation of motion ;
Rouse :	$2.4 < \dfrac{w_s}{u_*} < 3.6$	bed-load transport ;

$$\mathrm{Sh}_c = 0.062 \text{ (Paphitis, 2001)}$$

Methodology debrief

For flow dynamics

- determination of friction velocity u_* based on theoretical turbulent profile ; assumption $u_*(t) = F\{< u > (y_0, t)\}$; correction of results based on global values (contact needle) ;
- Obtaining of time-dependent friction velocity $u_*(t)$.

For sediment transport

- Image acquisition from fast-recording camera ; images processing on Matlab ; PTV algorithm ; correction of particles size/velocities ; time dependent discharge computation ; comparison to global values from mean weighted discharge ;
- Obtaining of time-variable transport rate $q(t)$.

Methodology debrief

For flow dynamics

- determination of friction velocity u_* based on theoretical turbulent profile ; assumption $u_*(t) = F\{< u > (y_0, t)\}$; correction of results based on global values (contact needle) ;
- Obtaining of time-dependent friction velocity $u_*(t)$.

For sediment transport

- Image acquisition from fast-recording camera ; images processing on Matlab ; PTV algorithm ; correction of particles size/velocities ; time dependent discharge computation ; comparison to global values from mean weighted discharge ;
- Obtaining of time-variable transport rate $q(t)$.

Methodology debrief

For flow dynamics

- determination of friction velocity u_* based on theoretical turbulent profile ; assumption $u_*(t) = F\{< u > (y_0, t)\}$; correction of results based on global values (contact needle) ;
- Obtaining of time-dependent friction velocity $u_*(t)$.

For sediment transport

- Image acquisition from fast-recording camera ; images processing on Matlab ; PTV algorithm ; correction of particles size/velocities ; time dependent discharge computation ; comparison to global values from mean weighted discharge ;
- Obtaining of time-variable transport rate $q(t)$.

Statistically...

$$q(t) \stackrel{?}{=} f\{u_*(t)\}$$

Friction velocity obtaining

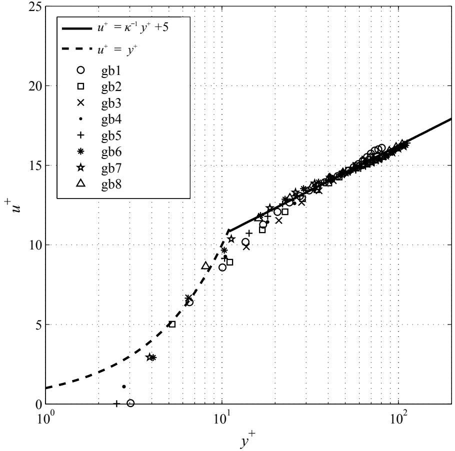

In wall coordinates :
$u^+ = u(y)/u_*$
and
$y^+ = u_* y/\nu$

For viscous sublayer :
$u^+ = y^+$;
For log region :
$u^+ = \kappa^{-1} \log y^+ + 5$;

Figure 7 – Turbulent characteristics of average profile of mean flow velocity. Lines indicate theoretical values : solid line is $u^+ = \kappa^{-1} \log y^+ + 5$ for log region ; dashed line is $u^+ = y^+$ for viscous layer.

Turbulent intensities - u^+_{RMS}

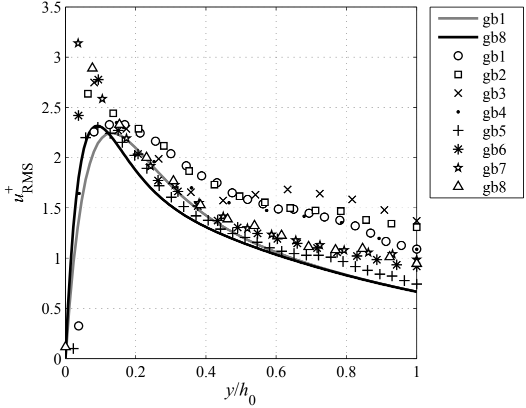

(Antonia and Krogstad, 2001)

$$u^+_{\mathrm{RMS}} = A \exp\left(-\frac{y^+}{Re_*}\right)\left[1 - \exp\left(-\frac{y^+}{B}\right)\right] + Cy^+ \exp\left(-\frac{y^+}{B}\right)$$

$A = 2$, $B = 8$, and $C = 0.34$;
$Re_* = u_{*\mathrm{PIV}} h_0/\nu$ is the Reynolds number using friction velocity as reference.

Figure 8 – Turbulent intensities for runs gb1 to gb8. Lines indicate computed values following empirical results from Antonia and Krogstad (2001). Longitudinal turbulent intensities u^+_{RMS}; dark line represent run computed value for gb1, and gray line, for gb8.

Friction velocity $u_*(t)$

Bottom shear stress :
$\tau_b \sim \rho u_*^2 \sim \rho g h_0 \sin\theta$

For our experiments :

- $u_* \sim 0.01\ \mathrm{ms}^{-1}$;
  $\rightarrow \tau_b \sim (10^3)(10^{-2})^2 \sim 0.1$ Pa ;
- $h_0 \sim 0.01$ m ;
  $\rightarrow \tau_b \sim (10^3)(10^1)(10^{-2})(10^{-2}) \sim 1$ Pa ;

The precision required to measure fluctuations would be ~ 0.01 Pa

! ! !

(Detert et al., 2010; Amir et al., 2014)

So, an indirect measure is pursued...

Friction velocity correlation

$\tau_b(t)$?

- $u_*^2 \propto \tau_b \propto u_0^2$
- $u(y_0) \propto u_0 \rightarrow u_* \propto u(y_0)$

  Dimensionally and statistically we can assume that :
- $\bar{u}_*^2(t) \propto \bar{\tau}_b(t) \propto \bar{u}^2(y_0, t)$
- so there is a function F that : $\bar{u}_*(t) = F\{\bar{u}(y_0, t)\}$

  (Ould Ahmedou et al., 2007)
- the hypothesis : F is also valid for instantaneous variables, so that : $u_*(t) = F\{u(y_0, t)\}$

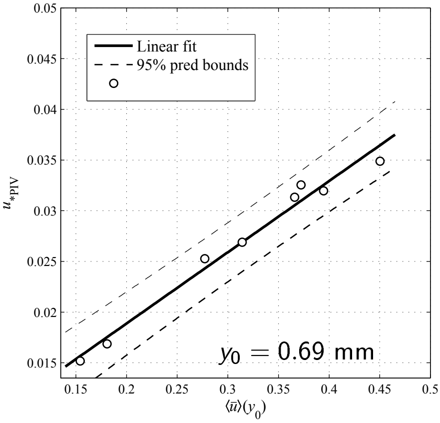

Figure 9 – Correlation between $\langle \bar{u} \rangle (y_0)$ and $u_{*\mathrm{PIV}}$. First-order polynomial approximation and 95% confidence boundaries.

Friction velocity correlation

$\tau_b(t)$?

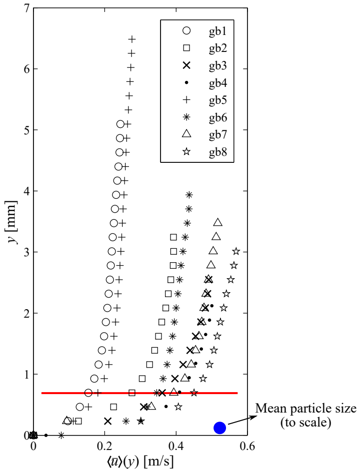

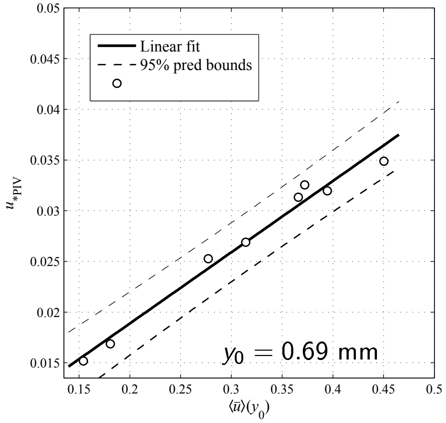

Figure 9 – Correlation between $\langle\bar{u}\rangle(y_0)$ and $u_{*\mathrm{PIV}}$. First-order polynomial approximation and 95% confidence boundaries.

Friction velocity signal

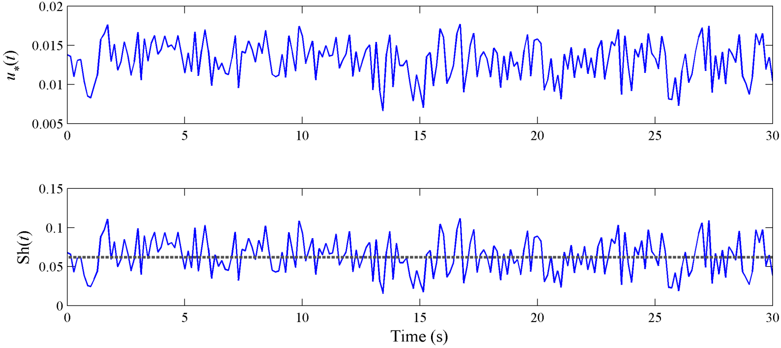

Figure 10 – Signals of $u_*(t)$ and $\mathrm{Sh}(t)$ for a close to threshold experiment run. The dotted dark line represent Sh_c.

Experimental project

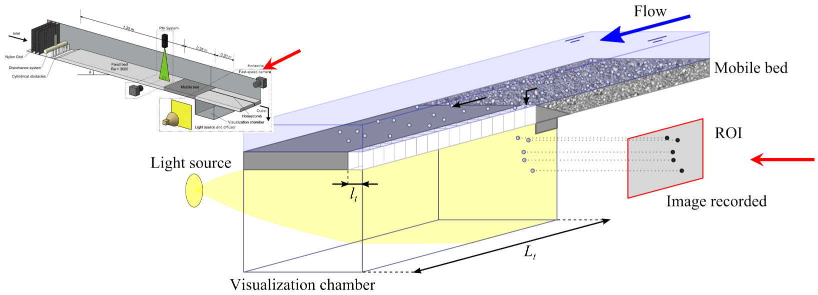

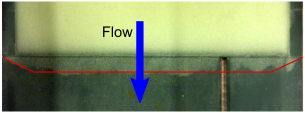

Top view of the trap.

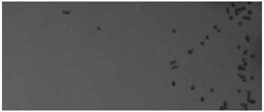

Side view, camera perspective.
(red arrow)

Experimental project

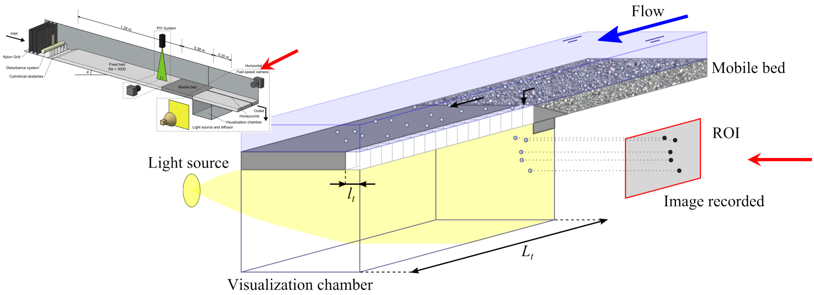

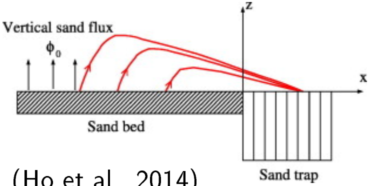

(Ho et al., 2014)

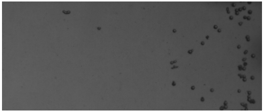

Side view, camera perspective. (red arrow)

Particles identification method

Original image

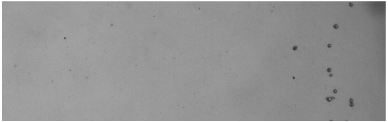

Linear histogram normalization

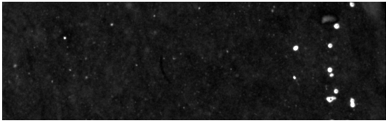

Binary Image

- Based on maximum and minimum images from series, each image gray level is adjusted ;
- Canny filter is applied, using Otsu's threshold method, to identify particle edges ;
- Morphological operations (closing, filling, opening, watershed) are performed.

(Frey et al., 2003)

Particle Tracking Velocimetry

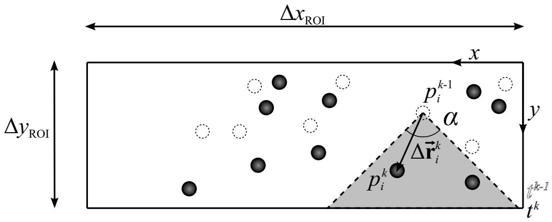

Particle mass :

$$m_i^k = \frac{\pi \rho_s}{6} {D_i^k}^3$$

Particle displacement :

$$\Delta \vec{r}_i^k$$

Particle velocity :

$$\vec{v}_i^k = \frac{\Delta \vec{r}_i^k}{\Delta t}$$

Total mass at time t^k :

$$M(t^k) = \sum_i^{N_p} m_i^k \,;$$

Time scale of particles permanence :

$$\Delta t_{\mathrm{esc}}^k = \frac{\Delta y_{\mathrm{ROI}}}{\bar{v}_{y_i}^k} \,;$$

Mean : $\bar{v}_{y_i}^k = \frac{1}{N_p} \sum_i^{N_p} v_{y_i}^k$;

Weighted-mean : $\bar{v}_{y_i}^k = \frac{1}{M(t^k)} \sum_i^{N_p} m_i^k v_{y_i}^k$.

Time dependent discharge :

$$q(t^k) = \frac{M(t^k)}{\Delta t_{\mathrm{esc}}^k},$$

Instantaneous discharge measurement

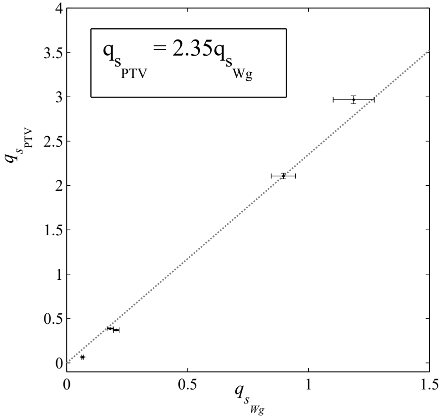

Figure 11 – Correlation between sediment discharge computation based on images and weighted mass.

Measure	u_*	Sh	Fr	$\bar{q}_{\mathrm{lW}}$	$\bar{q}_{\mathrm{lPTV}}$
gb1-2	0.014	0.068	1.16	0.065	0.064
gb1-3	0.014	0.075	1.20	0.179	0.386
gb1-4	0.015	0.079	1.10	0.204	0.336
gb2-1	0.021	0.158	1.55	1.187	2.967
gb2-2	0.021	0.159	1.54	0.896	2.107

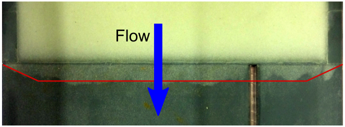

Top view of the trap.

$\mathrm{Sh} = 0.079, \mathrm{Fr} = 1.10$

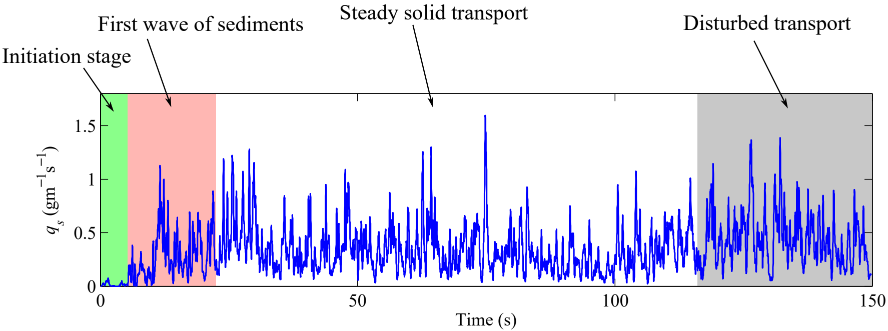

$\mathrm{Sh} = 0.079, \mathrm{Fr} = 1.10$

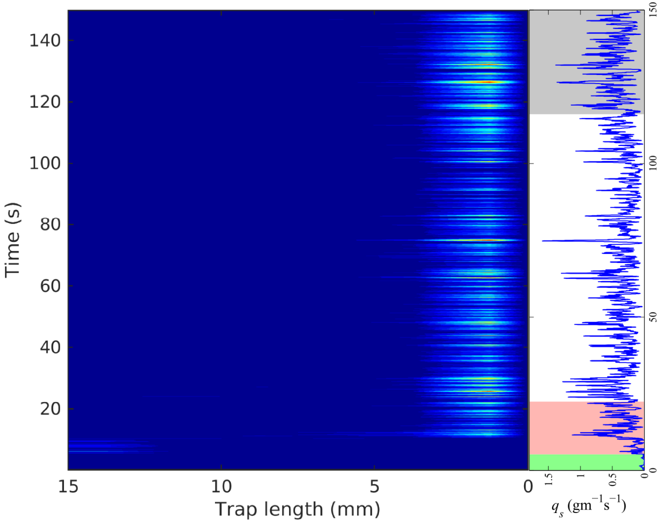

$\mathrm{Sh} = 0.159, \mathrm{Fr} = 1.54$

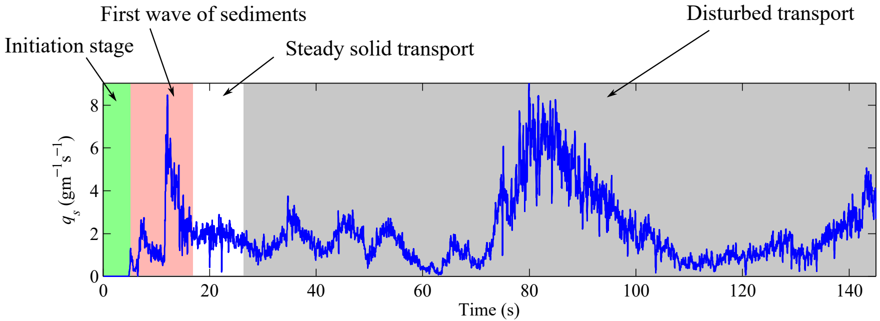

$\mathrm{Sh} = 0.159, \mathrm{Fr} = 1.54$

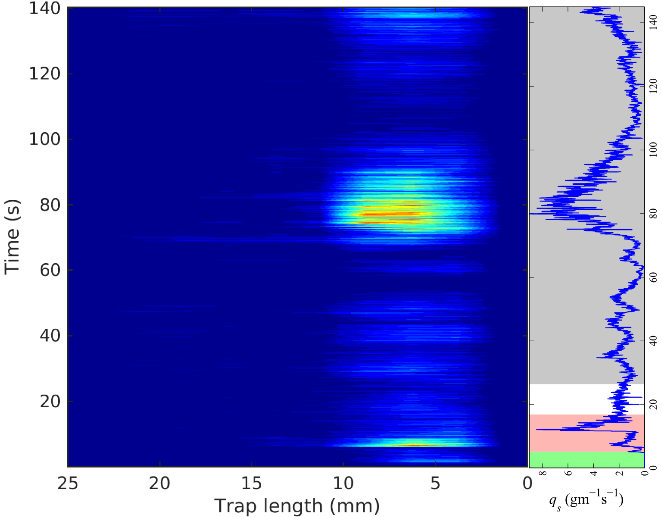

Comparison to classical formulas

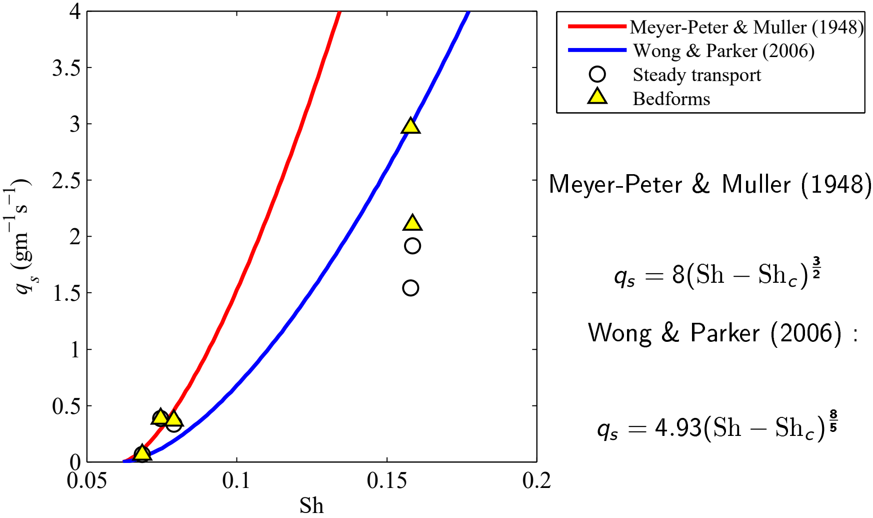

Meyer-Peter & Muller (1948) :

$$q_s = 8(\mathrm{Sh} - \mathrm{Sh}_c)^{\frac{3}{2}}$$

Wong & Parker (2006) :

$$q_s = 4.93(\mathrm{Sh} - \mathrm{Sh}_c)^{\frac{8}{5}}$$

PSD

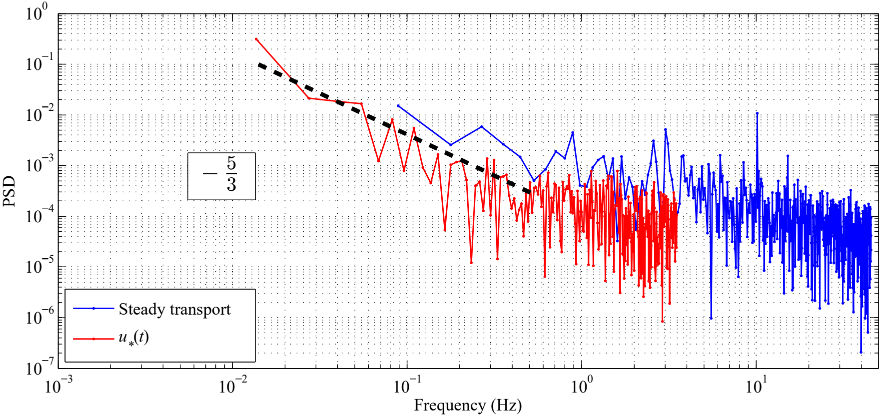

10^0
10^{-1}
10^{-2}
10^{-3}
10^{-4}
10^{-5}
10^{-6}
10^{-7}
PSD
$-\frac{5}{3}$
Steady transport
$u_*(t)$
10^{-3}
10^{-2}
10^{-1}
10^0
10^1
Frequency (Hz)

Discussions

- $q_{s\mathrm{RMS}}$ and $u_{*\mathrm{RMS}}$;
- characteristic time scales;
- additional effect : pulsating flows;

Thank you !

gfiorot@insa-rennes.fr
ghfiorot@gmail.com

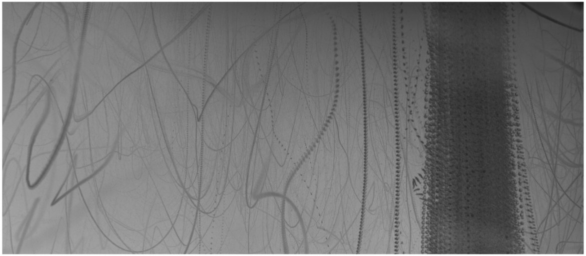

M. Amir, V. I. Nikora, and M. T. Stewart. Pressure forces on sediment particles in turbulent open-channel flow : a laboratory study. *Journal of Fluid Mechanics*, 757 :458–497, 2014. ISSN 0022-1120. doi : 10.1017/jfm.2014.498. URL http://www.journals.cambridge.org/abstract_S0022112014004984.

C. Ancey, a. C. Davison, T. Böhm, M. Jodeau, and P. Frey. Entrainment and motion of coarse particles in a shallow water stream down a steep slope. *Journal of Fluid Mechanics*, 595 (August), 2008. ISSN 0022-1120. doi : 10.1017/S0022112007008774.

R. A. Antonia and P.-r. Krogstad. Turbulence structure in boundary layers over different types of surface roughness. *Fluid Dynamics Research*, 28(2) :139, 2001. URL http://stacks.iop.org/1873-7005/28/i=2/a=A06.

A. A. Beheshti and B. Ataie-Ashtiani. Analysis of threshold and incipient conditions for sediment movement. *Coastal Engineering*, 55(5) :423–430, may 2008. doi : 10.1016/j.coastaleng.2008.01.003. URL http://linkinghub.elsevier.com/retrieve/pii/S0378383908000021.

M. Colombini and A. Stocchino. Coupling or decoupling bed and flow dynamics : Fast and slow sediment waves at high froude numbers. *Physics of Fluids*, 17 :036602(1–19), 2005.

T. R. H. Davies. Debris-flow surges - Experimental Simulation. *Journal of Hydrology*, 29(1) : 18–46, 1990.

M. Detert, V. Nikora, and G. Jirka. Synoptic velocity and pressure fields at the water-sediment interface of streambeds. *Journal of Fluid Mechanics*, 660 :55–86, 2010. ISSN 0022-1120. doi : 10.1017/S0022112010002545.

P. Frey, C. Ducottet, and J. Jay. Fluctuations of bed load solid discharge and grain size distribution on steep slopes with image analysis. *Experiments in Fluids*, 35(6) :589–597, 2003. ISSN 07234864. doi : 10.1007/s00348-003-0707-9.

T. D. Ho, a. Valance, P. Dupont, and a. Ould El Moctar. Aeolian sand transport : Length and height distributions of saltation trajectories. *Aeolian Research*, 12 :65–74, 2014. ISSN 18759637. doi : 10.1016/j.aeolia.2013.11.004.

E. Meyer-Peter and R. Müller. Formulas for bed-load transport. In *Proceedings of the 2nd Meeting of the International Association for Hydraulic Structures Research*, pages 39–64, Stockholm, 1948.

D. Ould Ahmedou, a. Ould Mahfoudh, P. Dupont, a. Ould El Moctar, a. Valance, and K. R. Rasmussen. Barchan dune mobility in Mauritania related to dune and interdune sand fluxes. *Journal of Geophysical Research : Earth Surface*, 112(2) :1–18, 2007. ISSN 21699011. doi : 10.1029/2006JF000500.

D. Paphitis. Sediment movement under unidirectional flows : an assessment of empirical threshold curves. *Coastal Engineering*, 43(3-4) :227–245, Aug. 2001.

A. Recking, P. Frey, A. Paquier, and P. Belleudy. An experimental investigation of mechanisms involved in bed load sheet production and migration. *Journal of Geophysical Research*, 114 (F3) :F03010, Aug. 2009. ISSN 0148-0227.

A. Shields. Application of Similarity principles and Turbulence Research to bed-load movement. *Mitteilungen der Preussischen Versuchsanstalt für Wasserbau und Schiffbau*, 1936. Original version in german (Anwendung der Aehnlichkeitsmechanik und der Turbulenz Forschung auf die Geschebebewegung).

M. Wong and G. Parker. The bedload transport relation of meyer-peter and müller overpredicts by a factor of two. *Journal of Hydraulics Engineering*, 132 :1159–1168, 2006.

Mean flow velocity and turbulent intensities

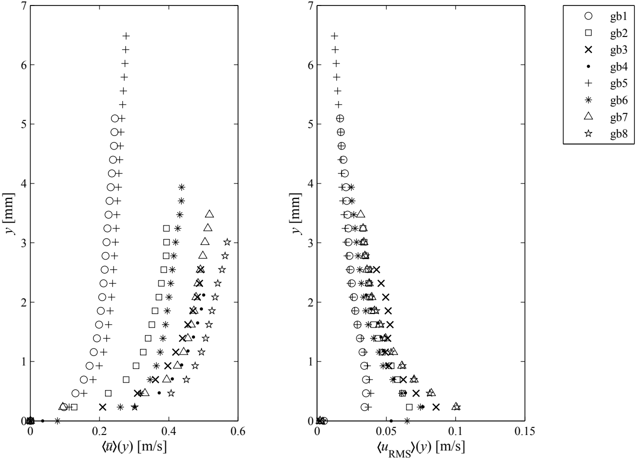

Figure 12 – Results for average profiles of mean flow velocity $\langle \bar{u} \rangle(y)$ and standard deviation $\langle u_{\mathrm{RMS}} \rangle(y)$ for runs gb1 to gb8.

Turbulent intensities - v^+_{RMS}

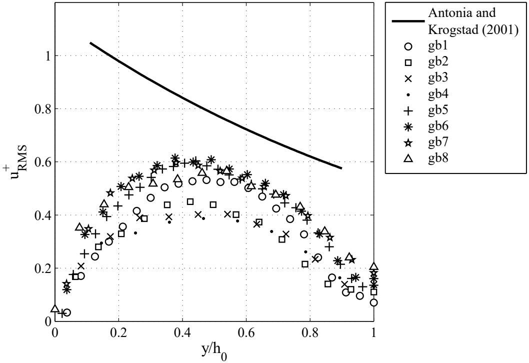

(Antonia and Krogstad, 2001)

$$v^+_{\mathrm{RMS}} = 1.14 \exp\left(\frac{-0.76y}{h_0}\right)$$

Figure 13 – Turbulent intensities for runs gb1 to gb8. Lines indicate computed values following empirical results from Antonia and Krogstad (2001). Vertical turbulent intensities v^+_{RMS} ; dark line represent computed values.

Friction velocity correction

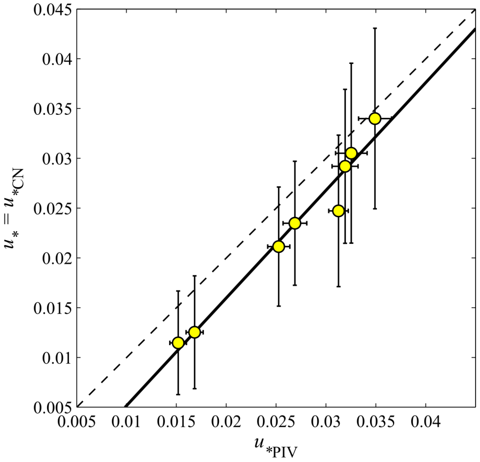

Figure 14 – Correlation between friction velocity computed through both methods $u_{*\mathrm{CN}}$ and $u_{*\mathrm{PIV}}$. Solid line represent linear relation between both methods for friction velocity calculation. Dashed line represents equality $u_{*\mathrm{PIV}} = u_{*\mathrm{CN}}$.

u_*

$u_* = u_{*\mathrm{CN}} = 1.08 u_{*\mathrm{PIV}} - 0.006$ with a correlation coefficient $R^2 = 0.96$.

Grain-size distribution

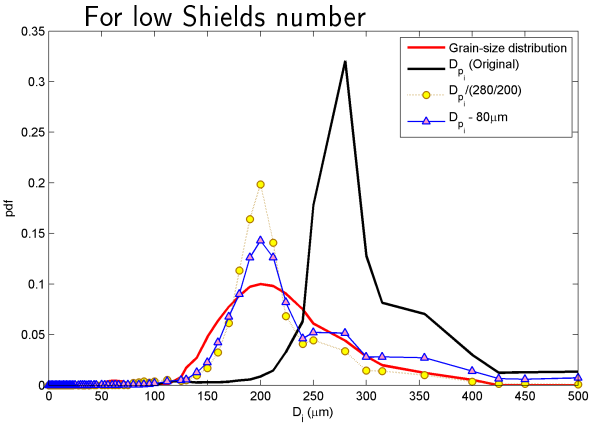

Figure 15 – Probability distribution function from captured images in comparison to calibrated grain-size distribution.

$\rightarrow$ Correction of particles diameter.

Δy_{ROI} influence

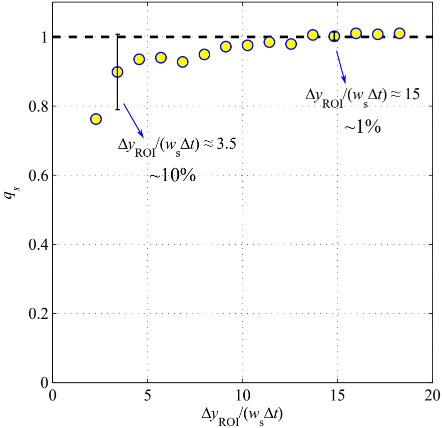

Figure 16 – Influence of Δy_{ROI} on $q_s(t)$.

Filtering of data, reducing discretization noise.

$\rightarrow$ Imposes time window of signal acquisition : Δt_{esc}.

In order to be comparable to PIV signal : $\Delta y_{\mathrm{ROI}} = 6.5\mathrm{mm}$

$(\Delta t_{\mathrm{esc}} = 0.13 - 0.14\mathrm{s})$

Δy_{ROI} influence

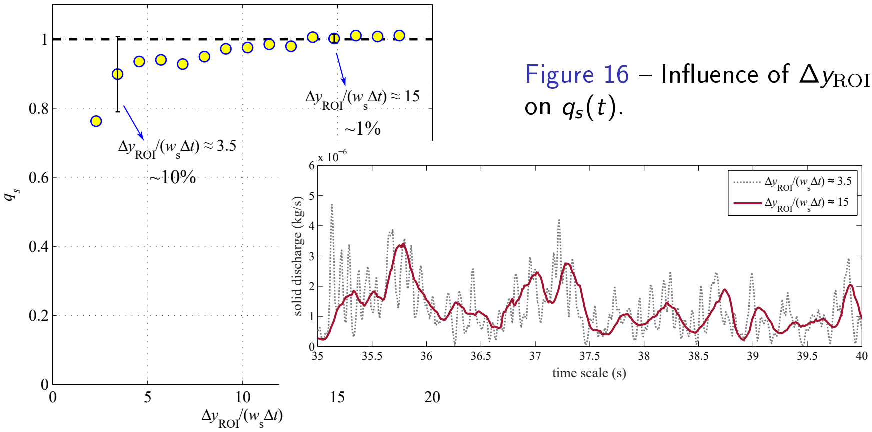

Figure 16 – Influence of Δy_{ROI} on $q_s(t)$.

$\rightarrow$ Imposes time window of signal acquisition : Δt_{esc}.

In order to be comparable to PIV signal : $\Delta y_{\mathrm{ROI}} = 6.5\mathrm{mm}$

$(\Delta t_{\mathrm{esc}} = 0.13 - 0.14\mathrm{s})$

Experimental run

1. arrange the experiment ;
2. partially block the outlet ;
3. set flow discharge and slope ;
4. start data acquisition (PIV and PTV) ;
5. release the outlet ;
6. after 1'30", data acquisition stops ;
7. block outlet ;

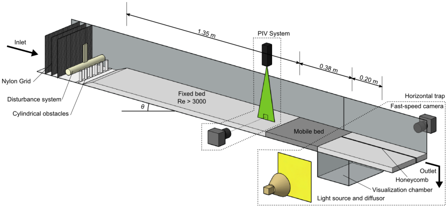

PSD

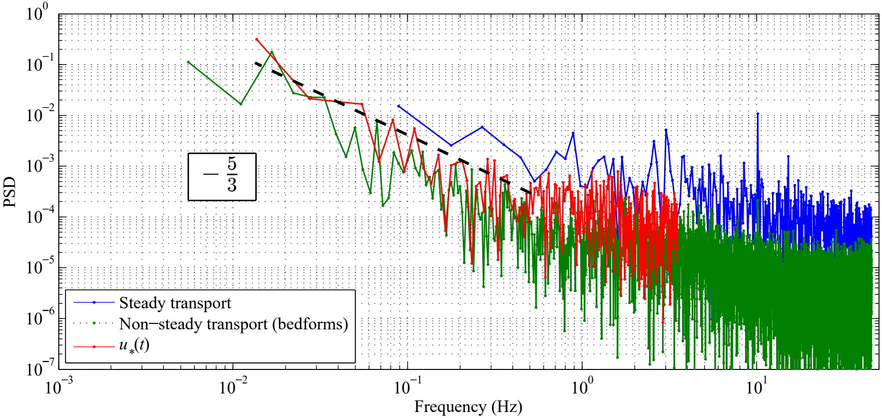
10^0
10^{-1}
10^{-2}
10^{-3}
10^{-4}
10^{-5}
10^{-6}
10^{-7}
PSD
10^{-3}
10^{-2}
10^{-1}
10^{0}
10^{1}
Frequency (Hz)
$-\frac{5}{3}$
Steady transport
Non−steady transport (bedforms)
$u_*(t)$